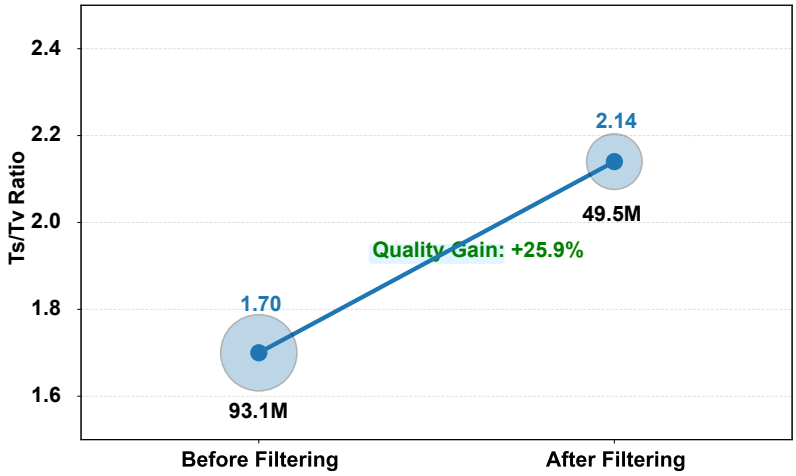


**Supplementary Fig. 1: Impact of genomic variant filtering on the transition-to-transversion (Ts/Tv) ratio and marker counts.**
Comparison of data quality metrics before and after applying population genetics hard filters to the raw cohort callset. The blue line tracks the upward shift in the overall Ts/Tv ratio from 1.70 to 2.14, capturing a 25.9% relative empirical gain in variant accuracy. Bubble areas are strictly proportional to the total number of SNPs retained in the dataset, which decreased from 93.1 million in the raw merged VCF to 49.5 million in the finalized biallelic filtered callset.

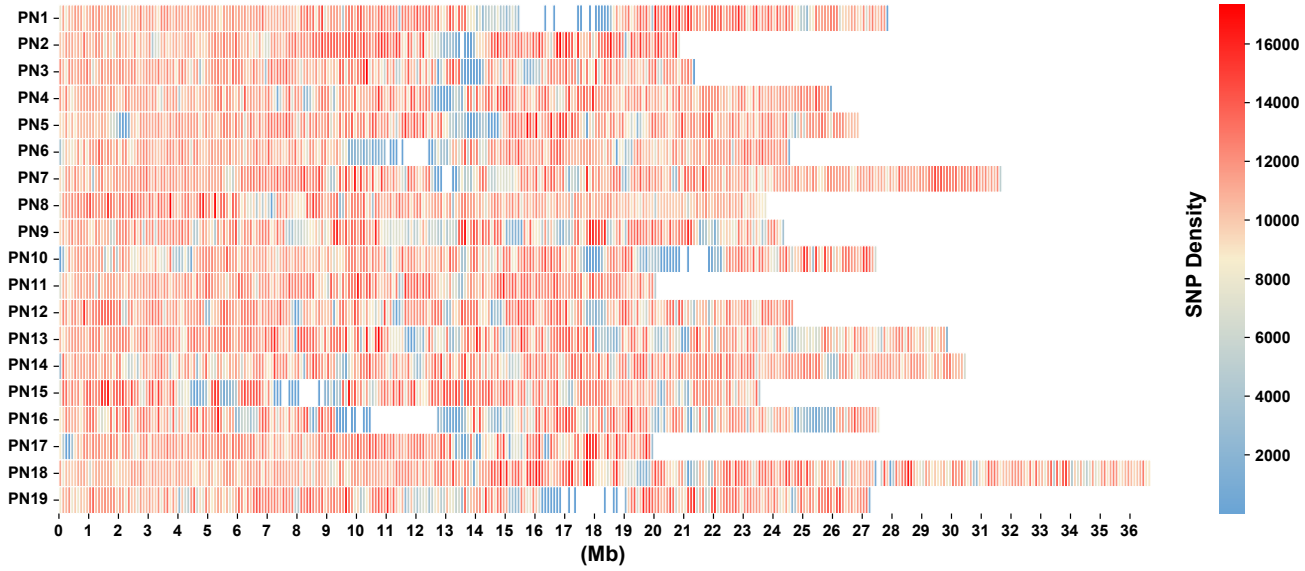


**Supplementary Fig. 2: Genome-wide SNP density distribution across the 19 grapevine chromosomes.**
Heatmap showing SNP density across the 19 primary autosomes of the *Vitis* reference genome. The horizontal axis indicates physical positions in megabases (Mb). Marker density was calculated within contiguous 0.1-Mb windows, with each vertical block representing a single window. Density values are indicated by the color bar on the right, ranging from blue (low density, <1,000 SNPs per window) to red (high density, >16,000 SNPs per window). Density tracking is based on the baseline callset compiled from the 223 *Vitis* accessions.

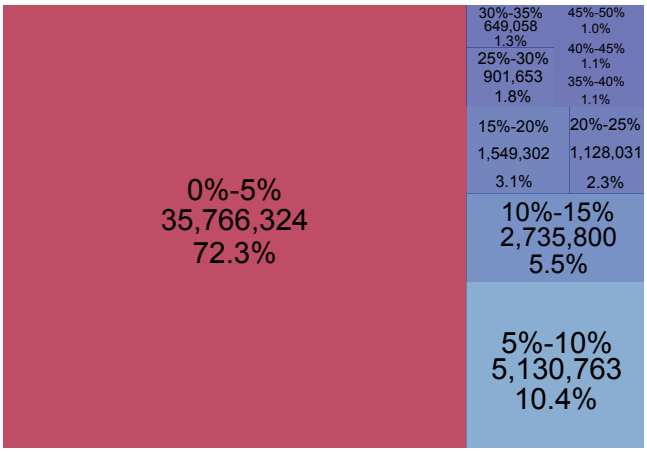


**Supplementary Fig. 3: Minor allele frequency (MAF) spectrum of the Vitis genomic variant dataset.**
Treemap showing the distribution of SNPs across specified MAF intervals based on the baseline callset from 223 *Vitis* accessions. The area of each rectangle is proportional to the total number of variants within that specific bin, with absolute variant counts and relative proportions (%) annotated inside each block. Rare variants (MAF 0–5%) constitute the largest reservoir of genetic diversity.

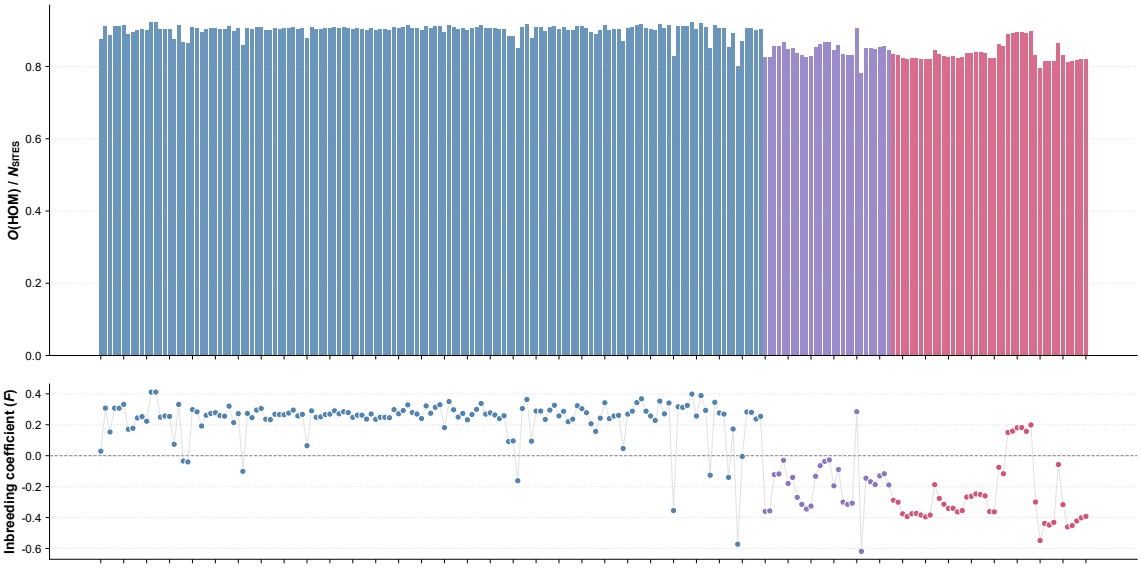


**Supplementary Fig. 4: Individual genomic homozygosity and inbreeding coefficients (*F*) across the *Vitis* accessions.**
The upper panel illustrates the observed proportion of homozygous sites ($O(\mathrm{HOM})/N_{\mathrm{SITES}}$) for each individual accession, visualized via a vertical bar plot. The lower panel depicts the corresponding inbreeding coefficient ($F$). Both metrics were calculated using the pre-imputation foundational dataset of dataset B. To maintain absolute consistency with the downstream framework, data points are presented exclusively for the finalized 216 core *Vitis* accessions, ensuring direct alignment with the population stratification and color-coding scheme inferred from the admixture analysis (**Fig. 1a**). Tick labels on the x-axis are sampled at a regular interval of five to maintain optimal legibility without spatial overlap.

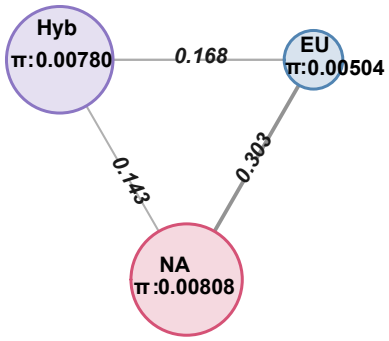


**Supplementary Fig. 5: Population genetic differentiation and diversity topology.**
Pairwise fixation index ($F_{ST}$) and nucleotide diversity ($\pi$) network across the three consolidated macro-cohorts: EUR, blue node, NAM, pink node, and HYB, purple node. Values printed inside the circular nodes indicate the average genome-wide nucleotide diversity ($\pi$) calculated for each consolidated group. Numerical values on the connecting edges indicate pairwise $F_{ST}$ coefficients, with line thickness strictly proportional to the genetic differentiation magnitude.

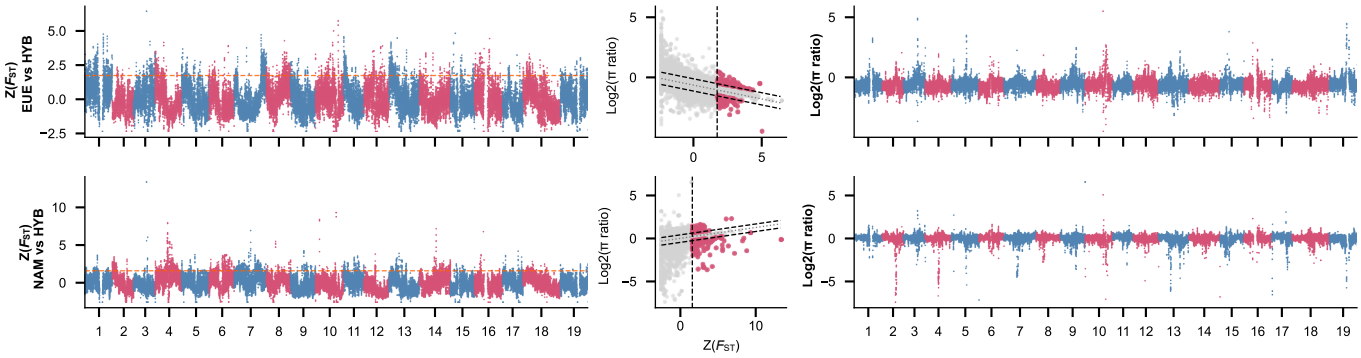


**Supplementary Fig. 6: Genome-wide selective sweep signatures and pairwise genetic differentiation involving the interspecific hybrid population.**
Pairwise selection scans for the comparisons of EUR against HYB (top panels) and NAM against HYB (bottom panels). For each comparison row, the layout displays the genome-wide *Z*-transformed $F_{ST}$ values across the 19 autosomes (left), the cross-validation scatter plots combining *Z*-transformed $F_{ST}$ and $\log_2(\pi$ Ratio) within 50-kb windows (middle), and the genome-wide $\log_2(P)$distributions across chromosomes (right). Colored dots in the scatter plots mark candidate regions exceeding selection thresholds.

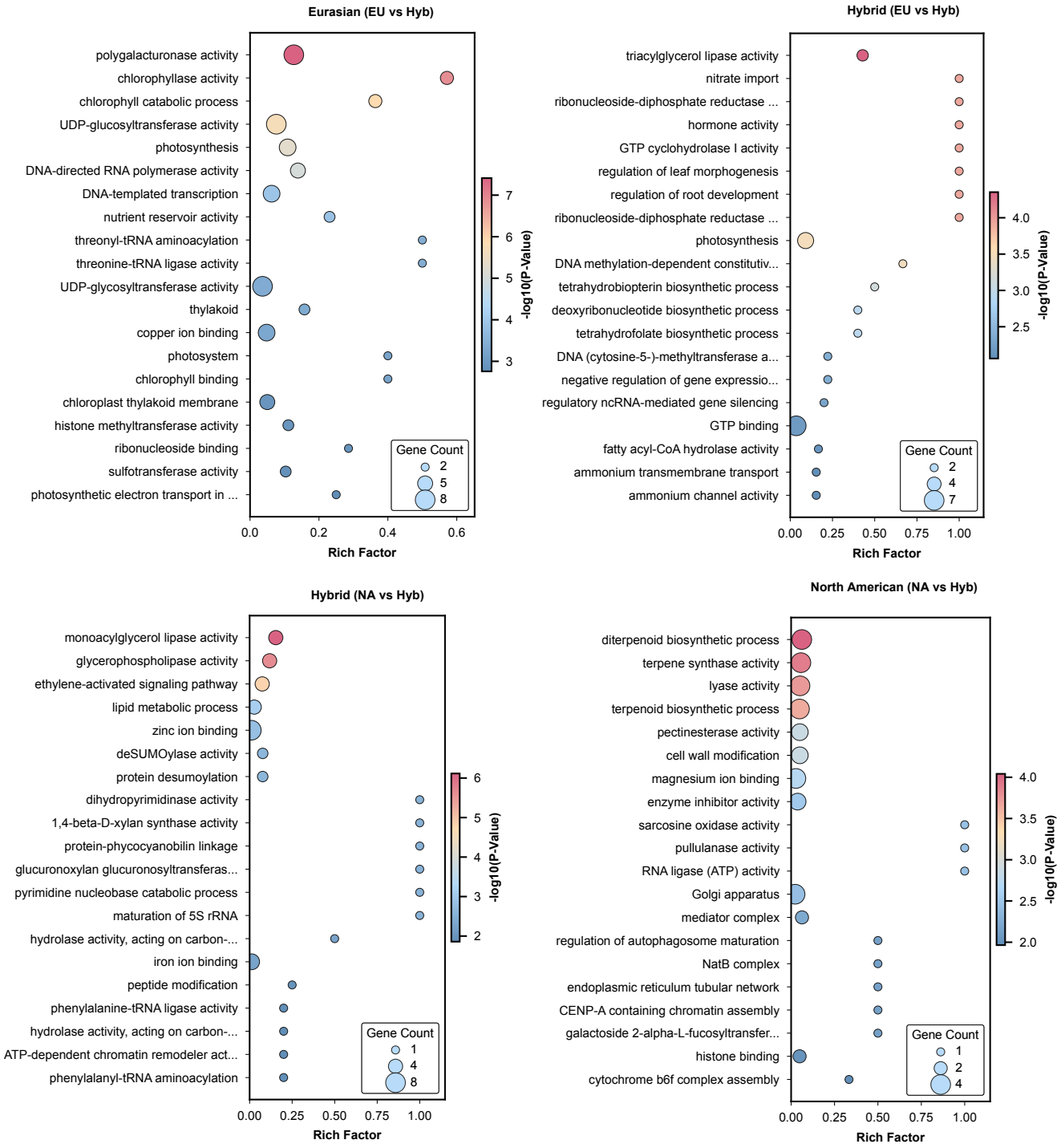


**Supplementary Fig. 7: GO enrichment profiles of candidate genes within joint $F_{ST}$ and $\pi$ selective sweep intersections.**

The four panels display the top 20 enriched functional terms for high-confidence candidate genes isolated from the intersection of pairwise $F_{ST}$ thresholds and $\log_2(\pi$ Ratio) empirical cutoffs.

Top row: GO terms enriched within selective windows from the comparison between the EUR and HYB, highlighting functional targets unique to the EUR lineage (top left) and the HYB pool (top right).

Bottom row: GO terms enriched within selective windows from the comparison between the NAM and HYB, highlighting functional targets unique to the HYB pool (bottom left) and the NAM lineage (bottom right).

Plot parameters: The horizontal axes indicate the Rich Factor, and the vertical axes list specific biological categories. Circular node sizes are proportional to the number of unique candidate genes mapping to each term (Gene Count), and node color shading indicates statistical significance scaled as $-\log_{10}(P\text{-value})$.

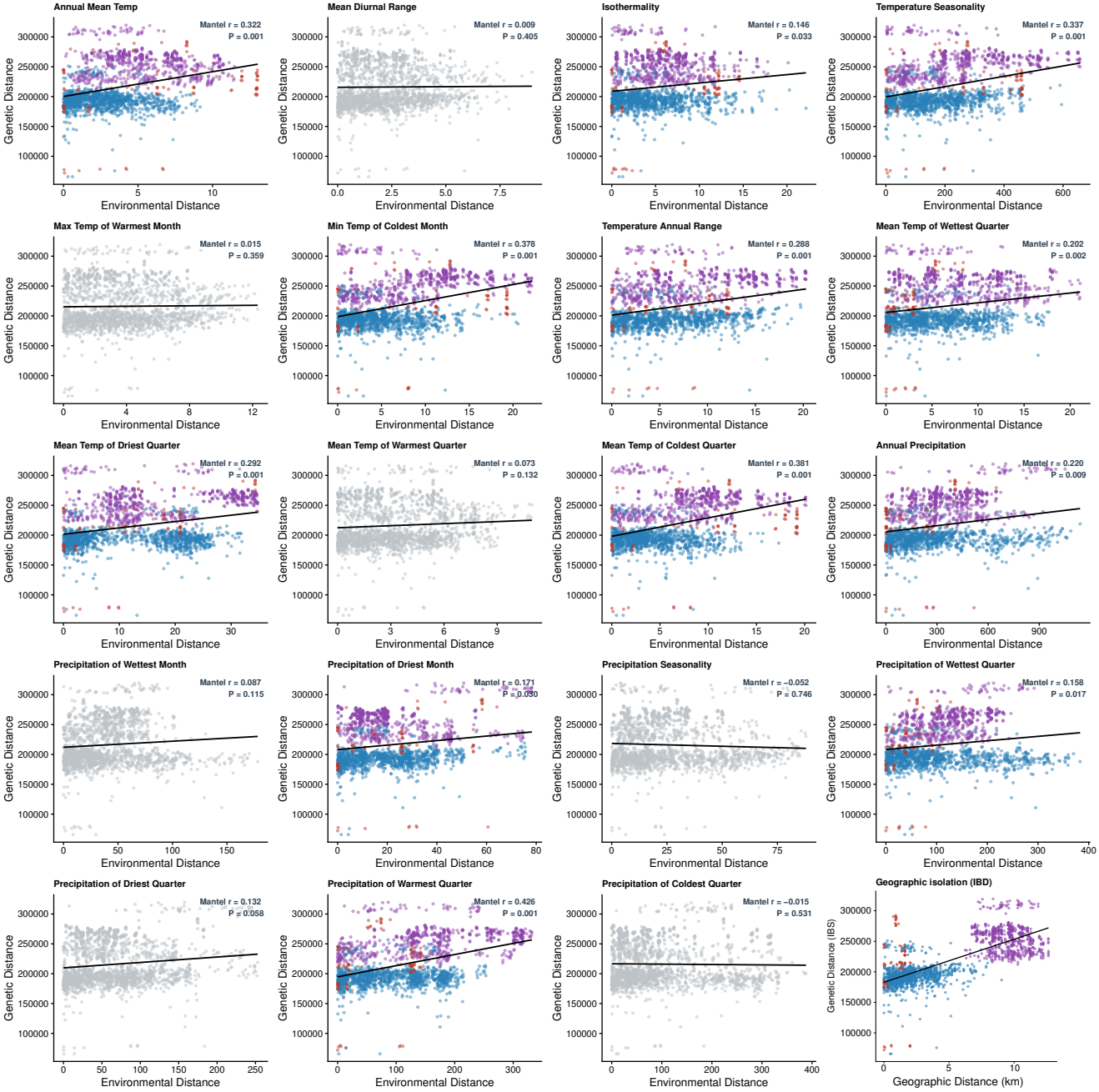


**Supplementary Fig. 8: Pairwise Mantel tests analyzing IBD and IBE models across *Vitis* accessions.**

Scatter plots display the mathematical relationships between pairwise genetic distance (vertical axes) and environmental distance or geographic distance (horizontal axes). The first 19 panels represent univariate environmental distance matrices derived individually from WorldClim bioclimatic variables (Bio1–Bio19), while the bottom-right panel represents isolation-by-distance based on geographic distance (km). Individual data points are color-coded by the lineage composition of each pairwise accession comparison: intra-EUR comparisons (blue), intra-NAM comparisons (red), and inter-clade EUR-NAM comparisons (purple). Panels plotted entirely in gray denote bioclimatic variables that failed to reach statistical significance ($P \geq 0.05$). The calculated Mantel correlation coefficient (Mantel $r$) and corresponding empirical $P$-value from permutation tests are annotated in the upper right corner of each individual panel.

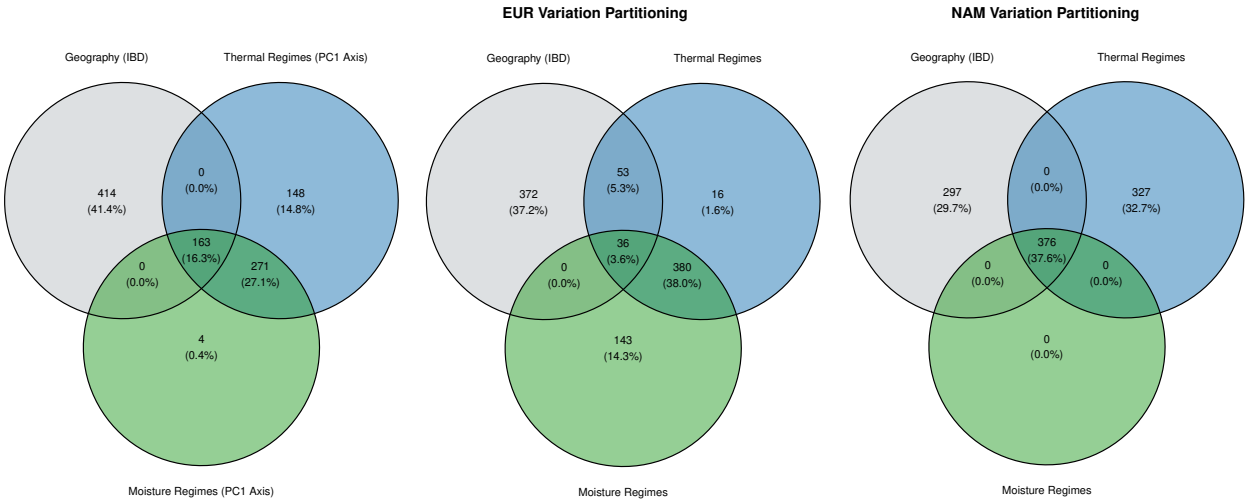


**Supplementary Fig. 9: VPA of geographic and macroclimatic factors driving adaptive genomic variation.**
Venn diagrams partition the relative contributions of geographic distance (IBD), temperature-related variables (Thermal Regimes),and moisture-related variables (Moisture Regimes) across a fixed pool of 1,000 environment-associated candidate loci. The three panels represent the total collection (left), EUR (middle), and NAM (right). Numerical annotations and corresponding percentages indicate the exact count and relative fraction (%) of adaptive variants uniquely or jointly explained by IBD and IBE components, scaling to a total of 1,000 loci per cohort.

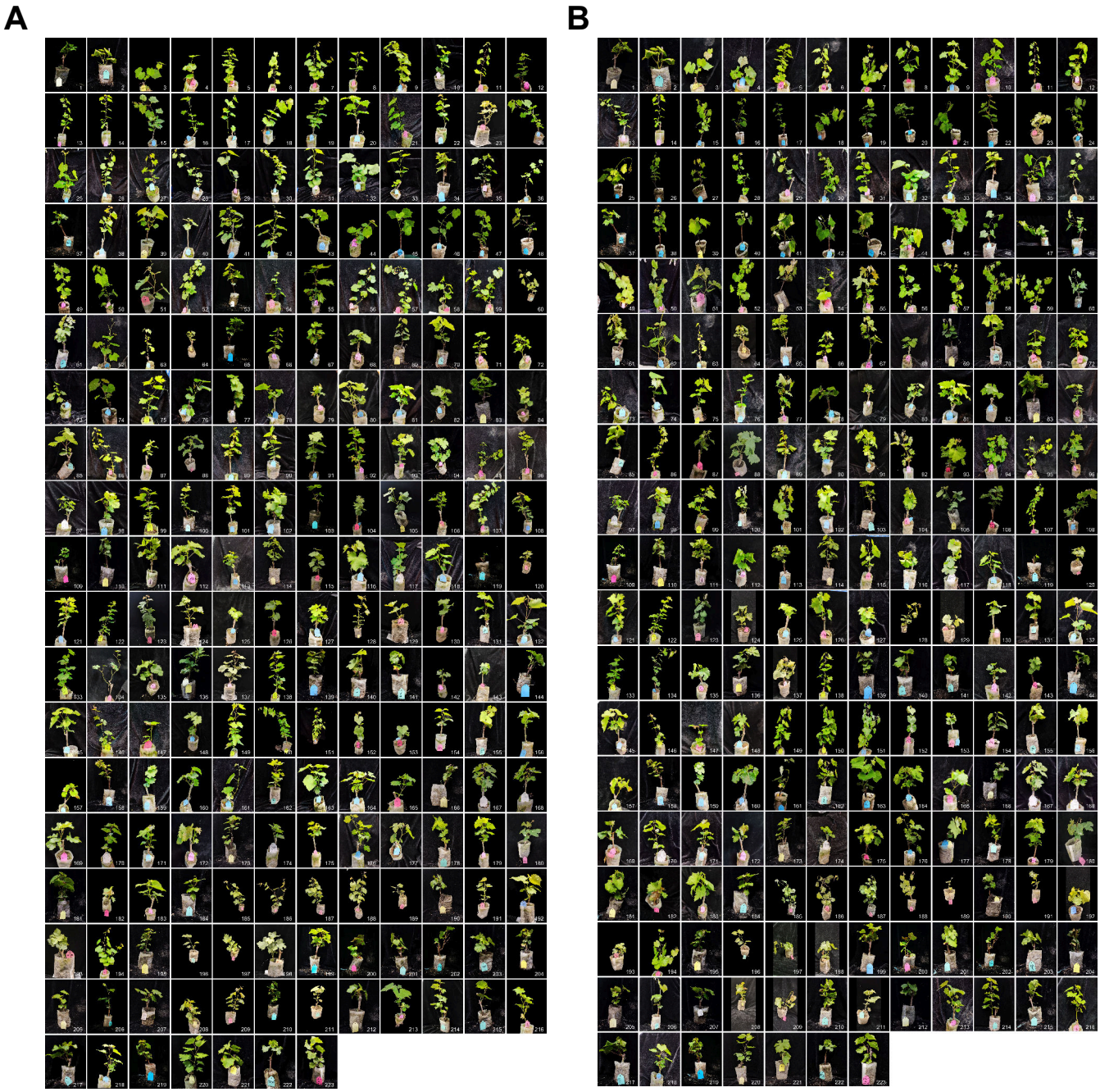


**Supplementary Fig. 10: Whole-plant phenotypes of the *Vitis* collection before and after cold stress.**

a, Macro-photographs of the 223 *Vitis* accessions under baseline control conditions (0 h).

b, Phenotypes of the identical individuals after 24 h of acute cold exposure.

Numbers in the bottom-right corners indicate the unique accession indices (1–223) cross-referenced to the germplasm metadata in Supplementary Data 1, Sheet 1.

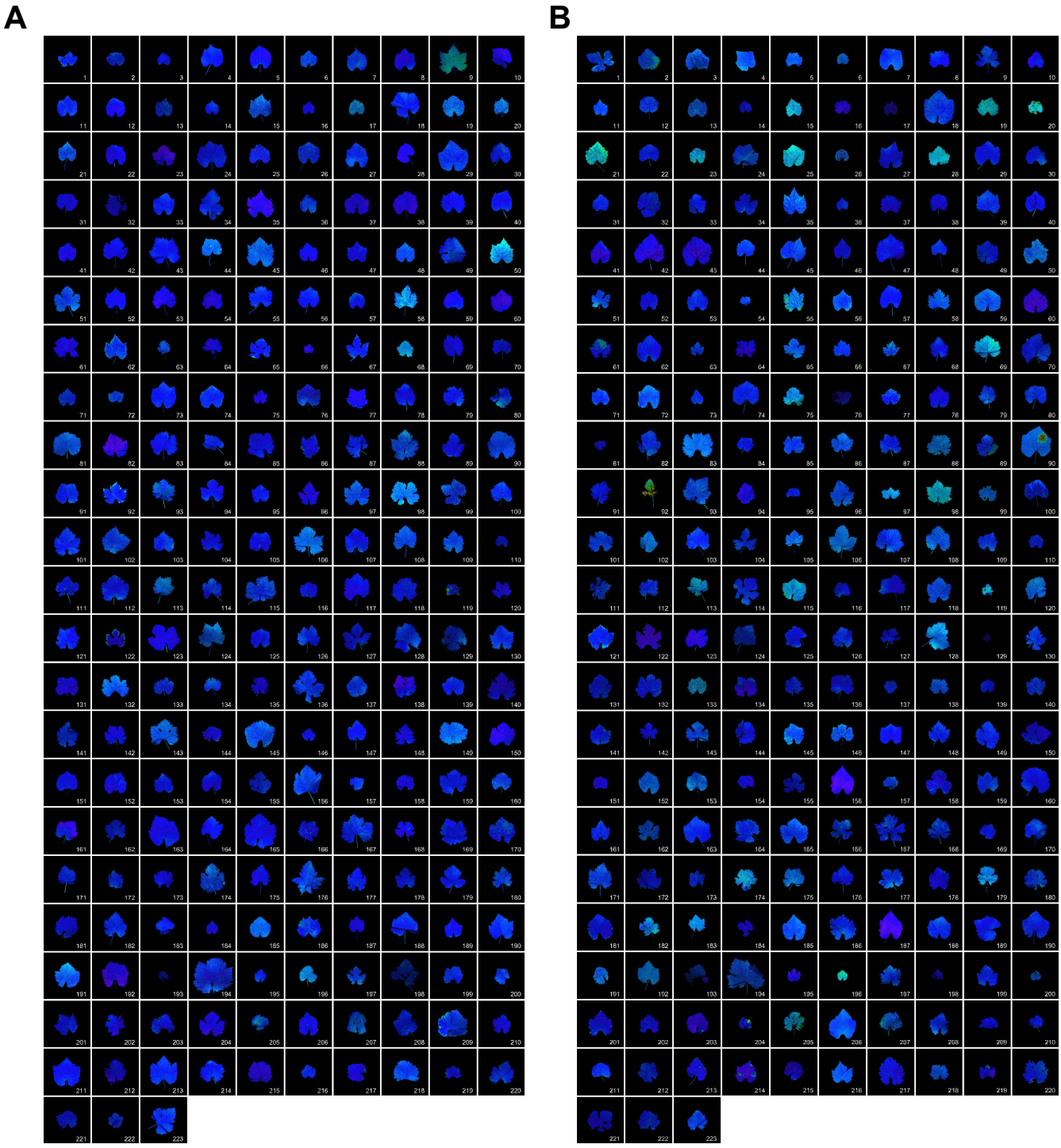


**Supplementary Fig. 11: *Vitis* chlorophyll fluorescence imaging (*F*v/*F*m) under control and cold stress.**

a, Chlorophyll fluorescence spatial mapping of the 223 *Vitis* accessions under baseline control conditions (0 h).

b, Spatial Fv/Fm imaging of the identical individuals following 24 h of cold stress.

*F*v/*F*m is spatially resolved by a false-color scale, where uniform dark blue indicates high, healthy values, and shifts to cyan, green, and yellow signal progressive photoinhibition and localized tissue damage. Numbers in the bottom-right corners correspond to accession indices (1–223) detailed in Supplementary Data 1, Sheet 1.

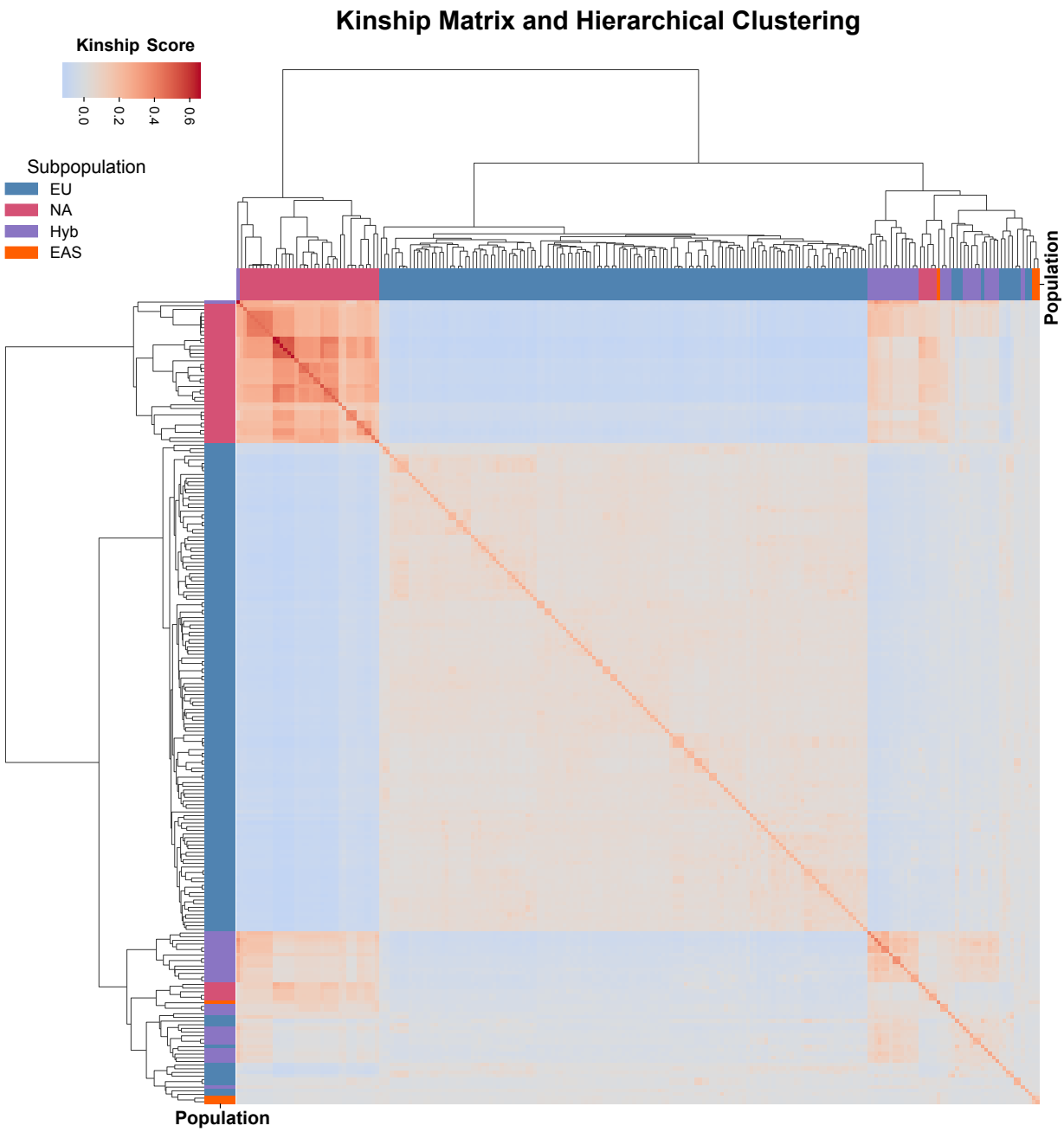


**Supplementary Fig. 12: Genome-wide kinship matrix and hierarchical clustering of the *Vitis* collection.**

Heatmap showing pairwise genetic relatedness coefficients (*K* matrix) calculated from the GWAS input variant callset to control for population stratification and cryptic relatedness. The color gradient represents kinship scores ranging from blue (low relatedness) to red (high relatedness). Top and left annotation tracks indicate subpopulation assignments: EUR (blue), NAM (pink), Hyb (purple), and East Asian clade (orange), bounded by marginal dendrograms illustrating hierarchical clustering based on genomic distance.

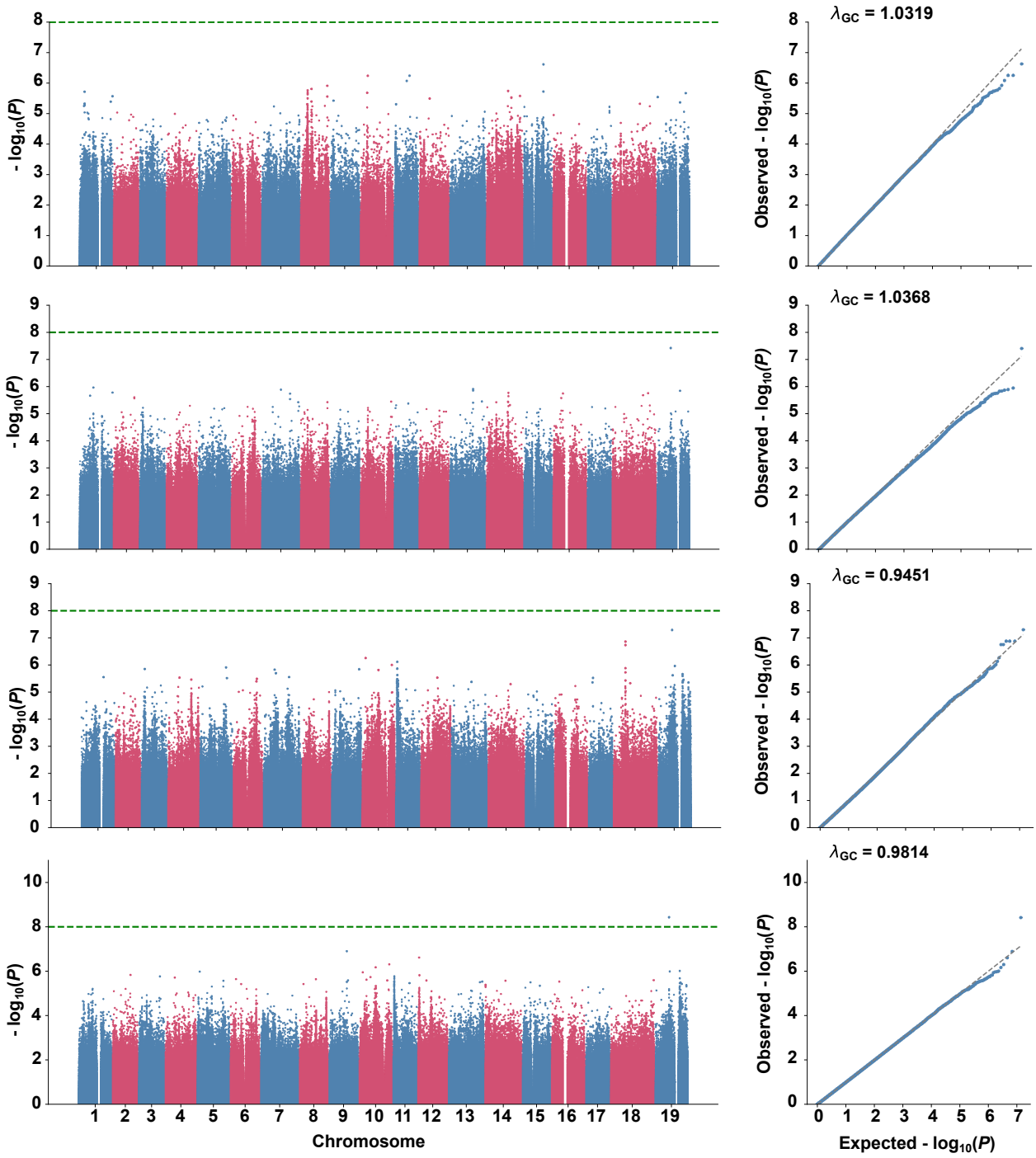


**Supplementary Fig. 13: GWAS landscapes for grapevine cold stress response across early time points.** Chronological tracking of association profiles for $F_v/F_m$ at 0, 2, 4,and 12 h of cold exposure (arranged sequentially from top to bottom rows). Left column displays manhattan plots across the 19 primary *Vitis* chromosomes, with the horizontal green dashed lines indicating the stringent genome-wide significance threshold ($-\log_{10}(P) = 8$). Right column displays corresponding quantile-quantile (Q-Q) plots of observed versus expected - $\log_{10}(P)$ values, with calculated genomic inflation factors ($\lambda_{GC}$) annotated to verify model calibration. The absence of sustained significant peaks at these early time points contrasts with the robust architecture captured at 24 h (Main Fig.4a).

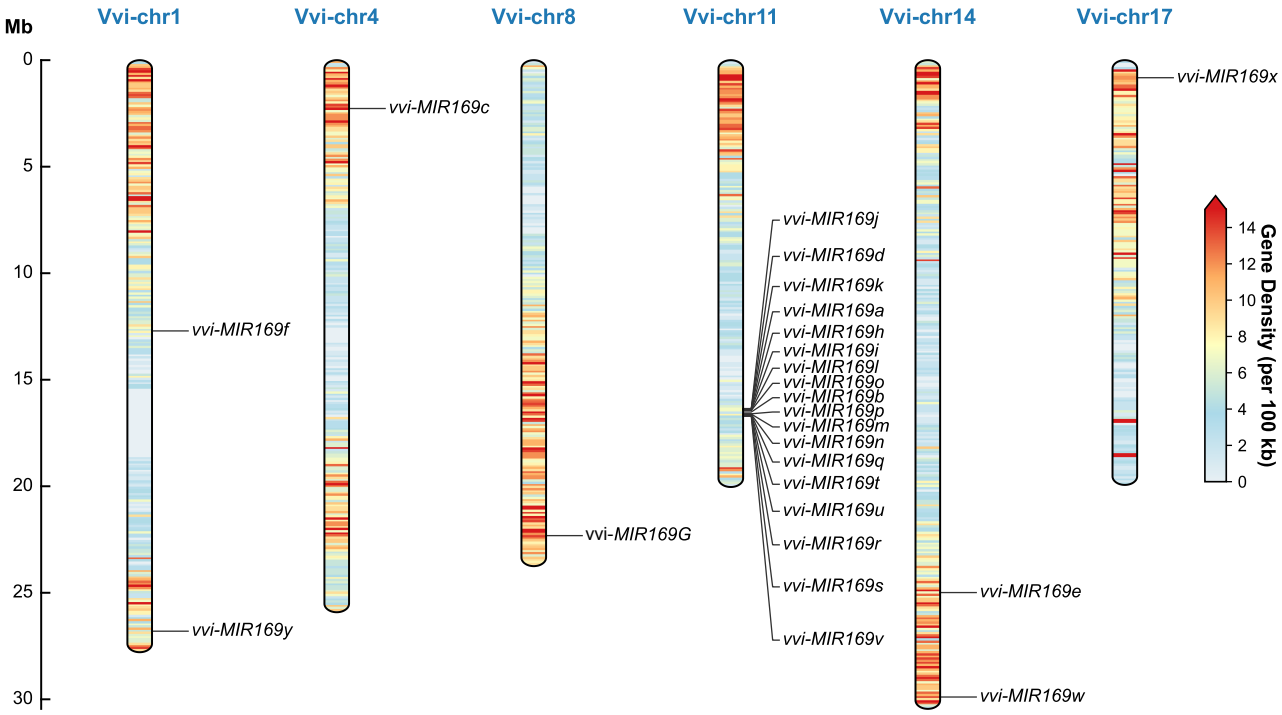


**Supplementary Fig. 14: Chromosomal localization of the *vvi-MIR169* family across the grapevine genome.**

Chromosomal mapping of the 25 identified *vvi-MIR169* precursors, with chromosome lengths drawn to scale (Mb). The internal heatmap illustrates background gene density (100-kb sliding windows) from light blue (low density) to dark red (high density, ≥ 14 genes/100 kb).

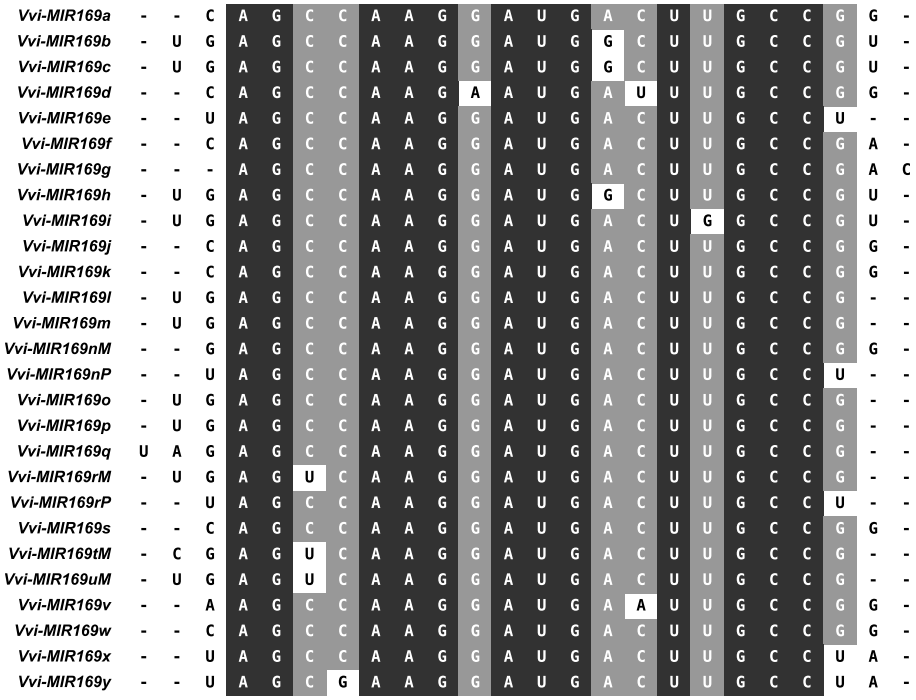


**Supplementary Fig. 15: Multiple sequence alignment of the mature vvi-*miR169* family members.**

Multiple sequence alignment illustrating the nucleotide conservation across the mature microRNA sequences of the 25 identified vvi-*miR169* family members. Shading intensity of nucleotides reflects their degree of sequence conservation.

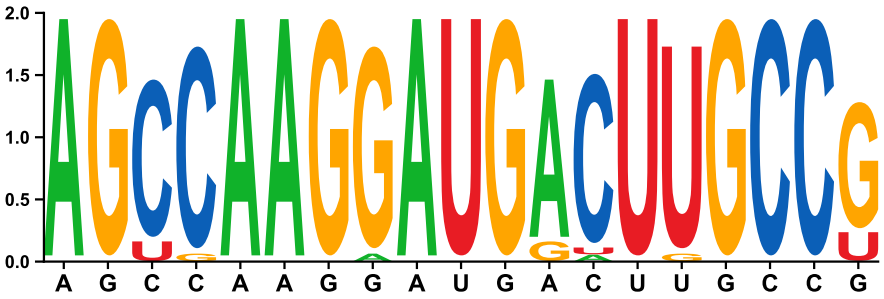


**Supplementary Fig. 16: Sequence logo of the mature vvi-*MIR169* miRNAs.**

The logo illustrates the nucleotide conservation across the core mature region of the vvi-*MIR169* family. The overall height of each stack indicates the sequence conservation at that position (measured in bits, with a maximum of 2.0 representing absolute conservation), while the height of individual letters reflects their relative frequency.

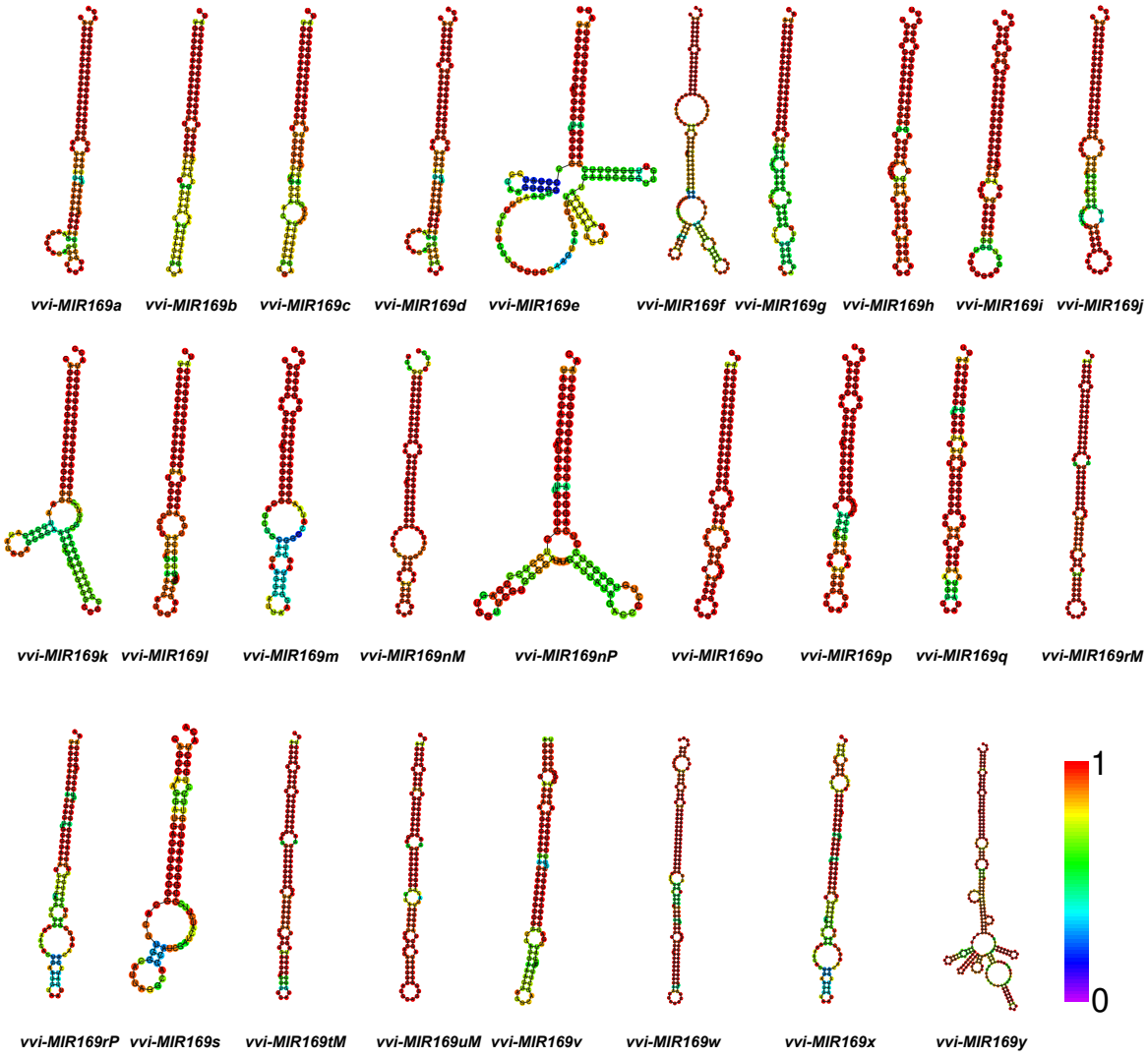


**Supplementary Fig. 17: Predicted secondary structures of the vvi-*MIR169* precursor miRNAs.**

The minimum free energy (MFE) structures of the 25 identified vvi-*MIR169* precursors were predicted using the RNAfold web server. The nucleotide color gradient encodes the calculated base-pairing probabilities,ranging from 0 (purple, low probability) to 1 (red, high probability). All family members fold into the canonical stem-loop (hairpin) structures characteristic of valid microRNA precursors, displaying highly stable double-stranded stem regions where the mature miRNAs are located.

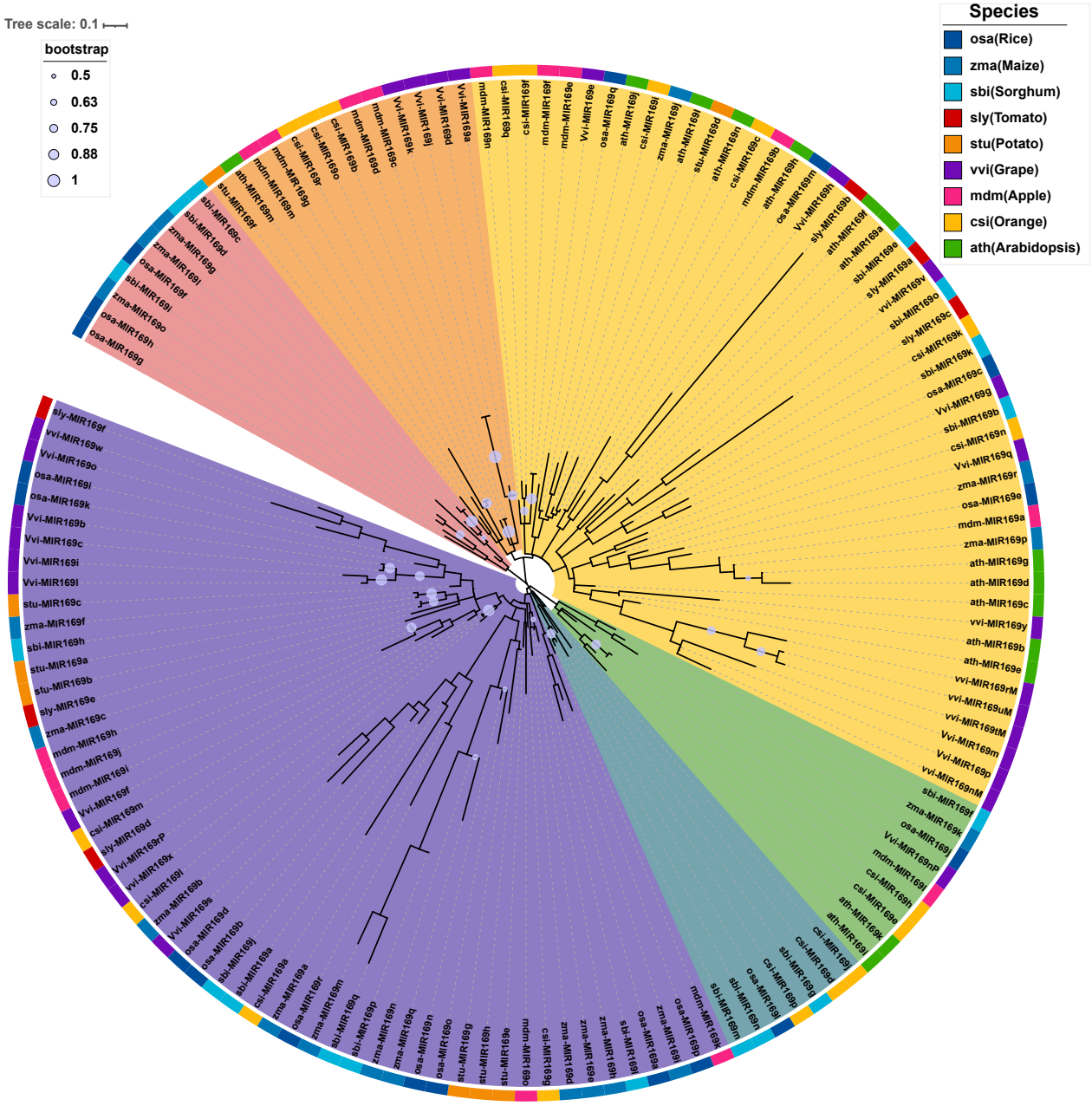


**Supplementary Fig. 18: Phylogenetic reconstruction of the *MIR169* precursor family across nine plant species.**

Unrooted maximum likelihood (ML) phylogenetic tree based on *MIR169* precursor sequences with 1,000 bootstrap replicates. The outer color strip designates the species of origin, encompassing three monocots (*Oryza sativa*, osa; *Zea mays*, zma; *Sorghum bicolor*, sbi) and six dicots (*Solanum lycopersicum*, sly; *Solanum tuberosum*, stu; *Vitis vinifera*, vvi; *Malus domestica*, mdm; *Citrus sinensis*, csi; *Arabidopsis thaliana*, ath). Internal colored sectors delineate six major evolutionary clades within the *MIR169* family. Purple circles at branch nodes indicate bootstrap support values ≥ 0.5, with circle size strictly proportional to the support value (range 0.5–1.0). The scale bar represents 0.1 nucleotide substitutions per site.

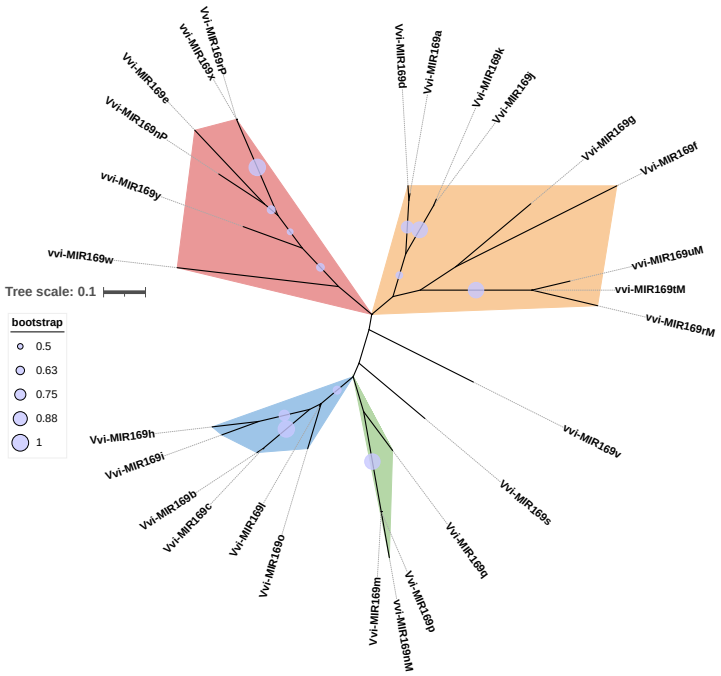


**Supplementary Fig. 19: Phylogenetic relationships of the vvi-*MIR169* precursor family in grapevine.**

Unrooted maximum likelihood (ML) tree constructed from the 25 identified vvi-*MIR169* precursor sequences. Distinct background polygons (red, orange, blue, and green) delineate four major evolutionary clades within the family. Purple circles at branch nodes denote bootstrap support values ≥ 0.5 (based on 1,000 replicates), with circle size strictly proportional to the confidence level (range 0.5–1.0). The scale bar indicates 0.1 nucleotide substitutions per site.

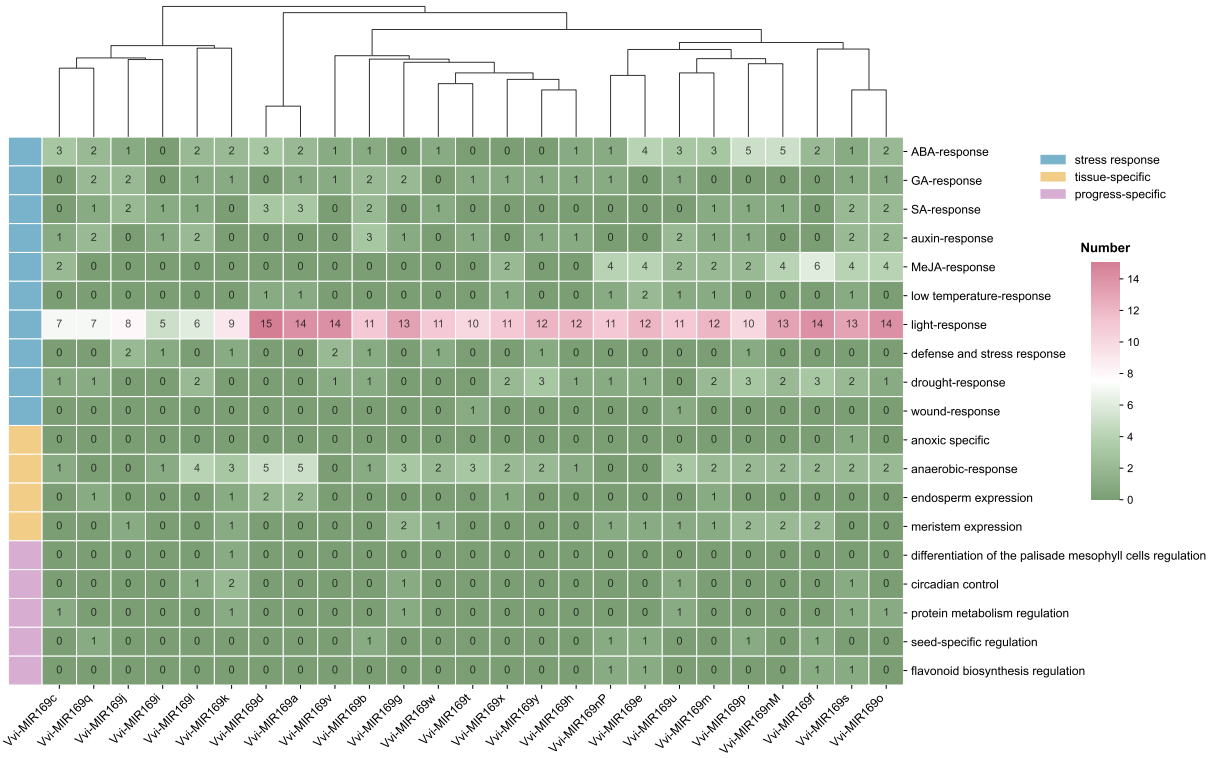


**Supplementary Fig. 20: Comprehensive profiling of cis-regulatory elements in the promoters of the *vvi-MIR169* family.**

Heatmap illustrating the distribution and frequency of identified cis-acting regulatory elements within the 2, 000 bp upstream promoter regions of the 25 vvi-*MIR169* precursors. The regulatory elements (rows) are classified into three major functional categories as indicated by the vertical color bar on the left. The color gradient from dark green to pink represents the absolute count of each motif within a given promoter. The widespread presence of stress-associated motifs, including low temperature-response (LTR) and ABA-response elements,underscores the extensive involvement of the *MIR169* family in grapevine environmental adaptation.

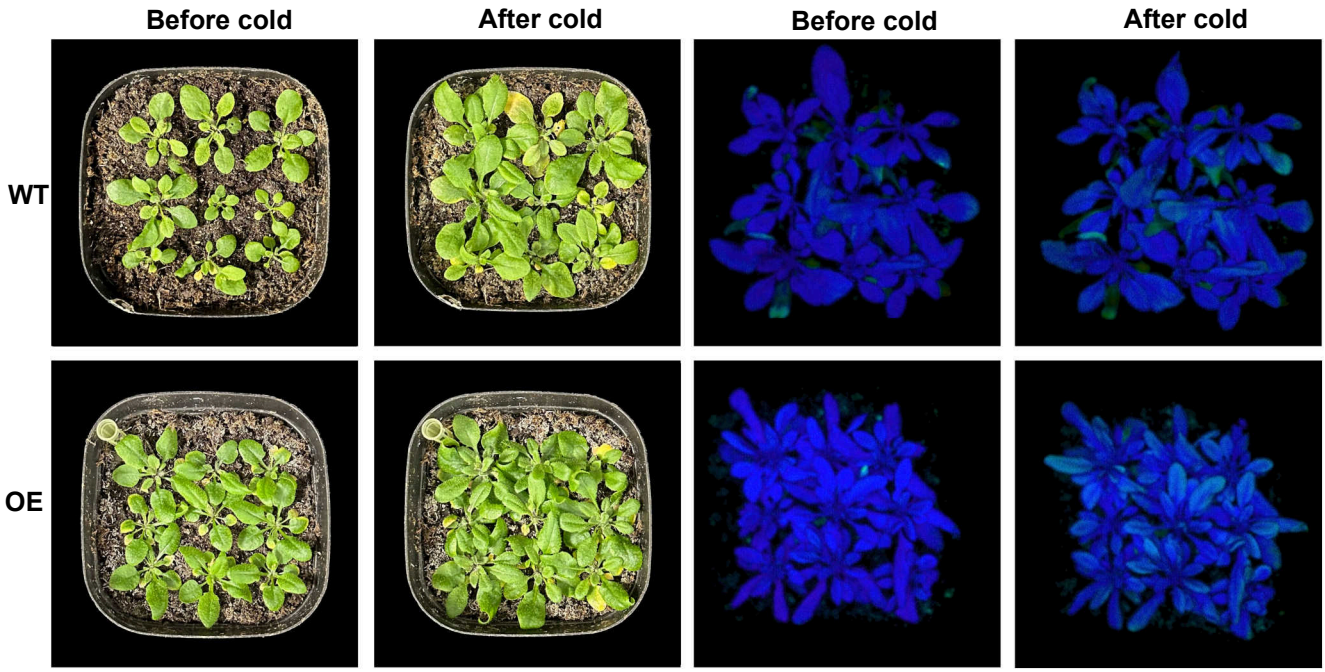


**Supplementary Fig. 21: Evaluation of cold-responsive phenotypes and photosynthetic efficiency in vvi-*miR169g*-OE *Arabidopsis* lines.**

Representative phenotypic and chlorophyll fluorescence images of wild-type (WT) controls and vvi-*miR169g*-OE *Arabidopsis* plants under normal conditions and cold stress. The panels from left to right show: visible light phenotypes before cold treatment, visible light phenotypes after cold treatment, initial chlorophyll fluorescence ($F_v/F_m$ imaging) before cold treatment, and $F_v/F_m$ imaging after cold treatment.